J|A|C|S
ARTICLES
Published on Web 03/07/2007

The Inconsistency in Adsorption Properties and Powder XRD Data of MOF-5 Is Rationalized by Framework Interpenetration and the Presence of Organic and Inorganic Species in the Nanocavities

Jasmina Hafizovic,[†] Morten Bjørgen,[†,||] Unni Olsbye,[†] Pascal D. C. Dietzel,[†] Silvia Bordiga,[‡] Carmelo Prestipino,[‡,§] Carlo Lamberti,[‡] and Karl Petter Lillerud*[,†]

Contribution from the Center for Materials Science and Nanotechnology, Department of Chemistry, University of Oslo, P.O. Box 1033 Blindern, N-0315 Oslo, Norway, and Dipartimento di Chimica, IFM and NIS Centre of Excellence, Via P. Giuria 7, I-10125 Torino

Received October 26, 2006; E-mail: k.p.lillerud@kjemi.uio.no

Abstract: MOF-5 is the archetype metal−organic framework and has been subjected to numerous studies the past few years. The focal point of this report is the pitfalls related to the MOF-5 phase identification based on powder XRD data. A broad set of conditions and procedures have been reported for MOF-5 synthesis. These variations have led to materials with substantially different adsorption properties (specific surface areas in the range 700 to 3400 m^2/g). The relatively low weight loss observed for some as synthesized samples upon solvent removal is also indicative of a low pore volume. Regrettably, these materials have all been described as MOF-5 without any further comments. Furthermore, the reported powder XRD patterns hint at structural differences: The variations in surface area are accompanied by peak splitting phenomena and rather pronounced changes in the relative peak intensities in the powder XRD patterns. In this work, we use single-crystal XRD to investigate structural differences between low and high surface area MOF-5. The low surface area MOF-5 sample had two different classes of crystals. For the dominant phase, $Zn(OH)_2$ species partly occupied the cavities. The presence of Zn species makes the hosting cavity and possibly also adjacent cavities inaccessible and thus efficiently reduces the pore volume of the material. Furthermore, the minor phase consisted of doubly interpenetrated MOF-5 networks, which lowers the adsorption capacity. The presence of Zn species and lattice interpenetration changes the symmetry from cubic to trigonal and explains the peak splitting observed in the powder XRD patterns. Pore-filling effects from the Zn species (and partly the solvent molecules) are also responsible for the pronounced variations in powder XRD peak intensities. This latter conclusion is particularly useful for predicting the adsorption properties of a MOF-5-type material from powder XRD.

1. Introduction

Crystalline metal−organic frameworks (MOFs) exhibiting large surface area and porosity retention upon solvent removal have achieved considerable attention because of their potential applications in separation, catalysis, nonlinear optics, and gas storage.[1−7] Traditionally, MOF syntheses have been designed to yield high quality single crystals suitable for structural analysis. A diversity of methods have been adopted, and they often involve a slow introduction of the reactants to reduce the rate of crystallite nucleation, such as slow diffusion of one component solution into another through a membrane or an immobilizing gel, slow evaporation of a solution of the precursors, or layering of solutions. Fortunately, solvothermal techniques have been found to be a convenient replacement for these often time-consuming methods. However, if an increased yield is more desirable than a high crystal quality, the reaction times can be significantly reduced by increasing reactant concentration and by employing agitation.[8] The product formed under these conditions may or may not be exactly identical to those obtained from methods used to produce highly crystalline MOF materials.

The initial findings of reversible hydrogen adsorption[9,10] and thermal robustness[11] of MOF-5 have made it one of the most studied metal−organic frameworks. A broad set of conditions

[†] University of Oslo.
[‡] IFM and NIS Centre of Excellence.
[||] Present address: Haldor Topsøe A/S, Nymøllevej 55, DK-2800 Lyngby, Denmark.
[§] Present address: ESRF, 6 rue Jules Horowitz, BP220, F-38043, Grenoble CEDEX, France.

(1) Yaghi, O. M.; Davis, C. E.; Li, G. M.; Li, H. *J. Am. Chem. Soc.* **1997**, *119*, 2861−2868.
(2) Bordiga, S.; Lamberti, C.; Ricchiardi, G.; Bonino, F.; Damin, A.; Lillerud, K. P.; Bjorgen, M.; Zecchina, A. *Chem. Commun.* **2004**, 2300−2301.
(3) Fèrey, G. *Chem. Mater.* **2001**, *13*, 3084−3098.
(4) Zaworotko, M. J. *Angew. Chem., Int. Ed.* **2000**, *39*, 3052−3054.
(5) Eddaoudi, M.; Kim, J.; Rosi, N.; Vodak, D.; Wachter, J.; O'Keeffe, M.; Yaghi, O. M. *Science* **2002**, *295*, 469−472.
(6) Seo, J. S.; Wang, D.; Lee, H.; Jun, S. I.; Oh, J.; Jeon, Y. J.; Kim, K. *Nature* **2000**, *404*, 982−986.
(7) Huang, L.; Wang, H.; Chen, J.; Wang, Z.; Sun, J.; Zhao, D.; Yan, Y. *Microporous Mesoporous Mater.* **2003**, *58*, 105−114.
(8) Rosewell, J. L. C.; Yaghi, O. M. *Microporous Mesoporous Mater.* **2004**, *73*, 3−14.

 10.1021/ja0675447 CCC: $37.00

and procedures have been tried to obtain MOF-5 either in large scale or with particular crystallite size or to reduce synthesis time.[7,12] Yaghi and co-workers have reported several different synthesis methods for MOF-5, and all of them yield a product with a fairly large crystallite size, suitable for structure determination.[11,13] Huang et al. reported a synthesis strategy for fast formation of nanocrystalline MOF-5.[7] Synthesis procedures yielding nanocrystalline MOF-5 are indeed interesting owing to their practical simplicity and because they present an opportunity to vary the properties of MOF-5 (or related materials) in, for example, adsorption and catalysis. Furthermore, a significant cost reduction may also be obtained from these procedures by substituting the commonly employed *N*,*N*′-diethylformamide (DEF) with *N*,*N*′-dimethylformamide (DMF) as solvent. Naturally, the inherent challenge with a nanocrystalline material is the limited structure information provided by powder XRD. Very recently, Ni et al. presented a new microwave-assisted solvothermal synthesis approach, which allows MOF-5 crystals of uniform size (4 ± 1 μm) to be synthesized in less than a minute.[12]

On the basis of the similar or at least related powder XRD patterns, the products from all the synthesis procedures have been claimed to be the same MOF-5 phase. However, a scrutiny of the published powder XRD patterns reveals clear intensity differences, especially in the two first and most intense peaks. Substantial variations in the surface area (700−3400 m^2/g) of MOF-5 prepared according to the different procedures have also been reported, but without any further explanations.[7,10,14,15] In this work, Huang's synthesis procedure has been followed closely, and also modified slightly in order to obtain sufficiently large crystals of low surface area (700 m^2/g) MOF-5 suitable for single-crystal XRD characterization. The scope of the present work has been to understand why materials reported to represent the same phase have such dramatic discrepancies in surface areas, and furthermore to demonstrate that this insight allows a fast evaluation of MOF-5 materials from the powder XRD characteristics. Supporting techniques in this work have been thermogravimetric analysis coupled to a mass spectrometer (TG−MS), scanning electron microscopy (SEM), infrared spectroscopy (IR), temperature resolved powder X-ray diffraction (XRD), X-ray absorption near-edge structure (XANES), and extended X-ray absorption fine structure (EXAFS).

2. Experimental Section

2.1. Synthesis. All chemicals were obtained commercially (Fluka) and used without further purification. Synthesis of the MOF-5 material consisting of nanocrystals was performed according to ref 7. To obtain the same phase with microsized crystals, the original synthesis procedure was modified. The reactants molar ratio was not altered, but the crystallizations were carried out at an elevated temperature without adding base.

The preparation of microsized crystals was performed by mixing $Zn(NO_3)_2 \cdot 6H_2O$ (0.29 g, 1 mmol), 1,4-benzenedicarboxylic acid (H_2-BDC) (0.08 g, 0.5 mmol), and *N*,*N*′-dimethylformamide (DMF) (9.5 g, 130 mmol) at room temperature. The thus obtained mixture was sealed, placed in the oven at 120 °C, and left at this temperature for 21 h. Crystallization was carried out under static conditions. The resulting solid was filtered, repeatedly washed with DMF, and dried at room temperature. The samples were stored in a vacuum desiccator to avoid water adsorption.[16]

2.2. Characterization. Powder XRD patterns were obtained with Siemens Bruker AXS D-5000 instruments using Cu Kα1 radiation in Bragg−Brentano reflecting and Debye−Scherrer transmission geometry. A powder XRD pattern of the nanocrystalline MOF-5 (later referred to as MOF-5_n) was also recorded at beam line BM31 (λ = 0.79997 Å) at the European Synchrotron Radiation Facility (ESRF) in Grenoble, France. The beam line was equipped with a Si(111) water-cooled, double-crystal monochromator. More details on the data acquisition can be found elsewhere.[17] Rejection of the harmonics, $\lambda/3$ and so forth, transmitted by the monochromator and the analyzer crystals is achieved by setting the electronic windows on the detector electronics so that they accept only counts from the fundamental λ. Digitalization of diffraction patterns from references 1 and 13 was performed with DIGITIZE 1.39b software.[18] The structure of the microcrystalline MOF-5 (later referred to as MOF-5_m) was investigated by single-crystal XRD using both synchrotron and Mo radiation on different crystals from the same synthesis batch. The structure of the MOF-5 modification later referred to as MOF-5_m_Zn was determined by single-crystal XRD using a conventional Bruker D8 diffractometer with an Apex II detector and an Oxford Cryosystems Cryostream Plus cooler. A total of 1800 frames were collected (λ = 0.71073 Å, $\Delta\omega$ = 0.3°), covering one hemisphere of the reciprocal space. The exposure time was 25 s per frame for the first 600 frames and 15 s for rest of the data set. The structure of the interpenetrated MOF-5 (later referred to as MOF-5_m_int) was determined by single-crystal XRD using synchrotron radiation (λ = 0.38745 Å) and a Bruker CCD detector at beamline ID11 at ESRF. A total of 1300 frames were collected ($\Delta\omega$ = 0.3°, 1 s per frame) covering one hemisphere of the reciprocal space. Two data sets with identical instrument parameters were recorded on the same crystal. The data sets were collected at room temperature and at 300 °C. The crystal was removed from the DMF solution and placed in an open 0.5 mm quartz capillary. The intention was to compare a fully solvated crystal with a solvent free one, but the heating from the extremely intense beam at ID11 gave a partly solvated crystal in the first data set. The second data set was recorded with reduced beam intensity to avoid detector saturation observed in the first measurement. A Cu absorber was placed between the sample and the beam. Data reduction and empirical correction on all data sets were carried out using the programs SAINT+[19] and SADABS,[20] respectively. The structures were solved by direct methods and refined in the WinGX program package[21] using the program SHELX-97.[22]

A temperature resolved series of powder XRD patterns was recorded with a Siemens D500 diffractometer using Cu radiation. The instrument was equipped with β-filter and scintillator counter. Powder XRD patterns were collected in the temperature range 75−450 °C in steps of 25 °C.

(9) Rosi, N. L.; Eckert, J.; Eddaoudi, M., Vodak, D. T.; Kim, J.; O'Keeffe, M.; Yaghi, O. M. *Science* **2003**, *300*, 1127−1129.
(10) Roswell, J. L. C.; Millward, A. R.; Park, K. S.; Yaghi, O. M. *J. Am. Chem. Soc.* **2004**, *126*, 5666−5667.
(11) Li, H.; Eddaoudi, M.; O'Keeffe, M.; Yaghi, O. M. *Nature* **1999**, *402*, 276−279.
(12) Ni, Z.; Masel, R. I. *J. Am. Chem. Soc.* **2006**, *128*, 12394−12395.
(13) Yaghi, O. M.; Eddaoudi, M.; Li, H.; Kim, J.; Rosi, N. Patent WO 02/088148 A1, 2002.
(14) Eddaoudi, M.; Moler, D. B.; Li, H.; Chen, B.; Reineke, T. M.; O'Keeffe, M.; Yaghi, O. M. *Acc. Chem. Res.* **2001**, *34*, 319−330.
(15) Panella, B.; Hirscher, M. *Adv. Mater.* **2005**, *17*, 538−541.
(16) Greathouse, J. A.; Allendorf, M. D. *J. Am. Chem. Soc.* **2006**, *128*, 10678−10679.
(17) Palomino, G. T.; Bordiga, S.; Zecchina, A.; Marra, G. L.; Lamberti, C. *J. Phys. Chem. B* **2000**, *104*, 8641−8651.
(18) Danon, Y. *DIGITIZE*, version 1.39b; 1992.
(19) *SAINT+*, version 6.22; Bruker AXS: Madison, 2001.
(20) Sheldrich, G. M. *SADABS*, *Empirical Absorption Corrections Program*; University of Göttingen: Göttingen, Germany, 1997.
(21) Farrugia, L. J. *WinGX*, *An Integrated System of Windows Program for Solution, Refinement and Analysis of Single-Crystal X-ray Diffraction Data*, version 1.70.01; 2005.
(22) Sheldrick, G. M. *SHELXL-97*, A *Program for Crystal Structure Refinement*; University of Göttingen: Göttingen, Germany, 1997.

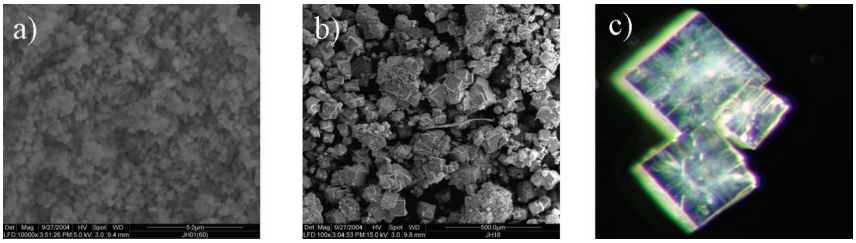

Figure 1. Microscopy images of (a) MOF-5_n (SEM), (b) MOF-5_m (SEM), and (c) MOF-5_m (light microscope).

Thermogravimetric (TG) analyses were carried out in flowing O_2 atmosphere (15 mL/min) with a heating rate of 5 °C/min, using a Rheometric Scientific STA 1500 instrument. The approximate sample weight was 10 mg. Scanning electron microscope (SEM) images were obtained in a Philips XL 30 scanning electron microscope. The samples were mounted on carbon tape.

X-ray absorption experiments on the Zn K edge were performed at BM29,[23] ESRF. The monochromator was equipped with two Si (311) flat crystals, and harmonic rejection was achieved using Rh coated mirrors after the monochromator. The following experimental geometry was adopted: (1) I_0 (10% efficiency); (2) MOF sample; (3) I_1 (50% efficiency); (4) reference; (5) I_2 (80% efficiency). This setup allows a direct energy/angle calibration for each spectrum avoiding problems related to energy shifts owing to the small thermal instability of the monochromator crystals.[24] Sampling steps of 0.2 eV and 0.025 $Å^{-1}$ were used for the XANES and EXAFS part, respectively. The measurements were performed in the range 9510 to 11180 eV, with an integration time of 3 s/point. The spectra were collected at room temperature using a metallic cell allowing in-situ high-temperature treatments and gas dosage.[25]

The EXAFS data analysis was performed using the EXTRA and FITEXA software, representing an evolution of the Frascati code.[26] The code exploits the fits in the *k*-space using the minimization routines of the MINUIT code.[27,28] Phase and amplitude functions were calculated by the FEFF 8.20 code[29] using the structure solved by single-crystal data as input, and they were verified with a ZnO model compound. The fit of EXAFS signals was carried out on back Fourier filtered signals, with a k^2 weight with *k* windows from 2.70 to 13.3 $Å^{-1}$, and filtering the signal in the range 1.1−3.60 Å: $2\Delta k\Delta R/\pi = 16.87$. This code has already been successfully used in the determination of the local environment of Cu(II) in HKUST-1 MOF.[30]

3. Results and Discussion

3.1. Powder XRD. The nanocrystalline MOF-5 (previously reported to have a low surface area compared to the original MOF-5 reported by Yaghi and co-workers) was prepared according to the direct mixing approach introduced by Huang et al.[7] The same phase consisting of microsized crystals, suitable for single-crystal structure analysis, was also prepared. The nanocrystalline and the microcrystalline MOF-5 samples are hereafter denoted MOF-5_n and MOF-5_m, respectively.

Figure 1 shows microscopy images of (a) MOF-5_n (SEM), (b) MOF-5_m (SEM), and (c) MOF-5_m (light microscope). The MOF-5_n crystals are too small for any evaluation of their actual size or shape. The crystallite size was, however, estimated from Scherrer's formula,[31] which suggested the crystallite size to be in the range 35−55 nm. SEM and light microscope images of MOF-5_m show cubically shaped crystals in the range 50−100 μm.

Figure 2 displays the powder XRD patterns of (a) MOF-5_m, (b) MOF-5_n, (c) digitalized powder XRD pattern of MOF-5 reported by Huang et al.,[7] (d) simulated powder XRD pattern of a MOF-5 crystal, and (e) digitalized powder XRD pattern of MOF-5 reported by Yaghi et al.[13] Figure 2 presents two rather important issues:

(1) The powder XRD patterns of MOF-5_m and MOF-5_n (Figure 2a,b) are in agreement with the pattern of the nanocrystalline MOF-5 reported by Huang et al.[7] (Figure 2c), strongly suggesting that they represent the same phase. Furthermore, N_2 adsorption measurements performed on MOF-5_n[32] and MOF-5_m gave Langmuir surface areas of 747 and 1104 m^2/g, respectively, which are close to the value measured by Huang et al. (722 m^2/g).[7] This implies that we have obtained microsized crystals of the low-surface-area MOF-5, giving us the possibility of attaining a deeper understanding of this material from single-crystal XRD (section 3.3).

(2) The experimental pattern obtained on a high-surface-area MOF-5 reported by Yaghi et al.[13] (Figure 2e) is consistent with the calculated MOF-5 pattern (Figure 2d). However, these two XRD patterns, representing the ideal MOF-5 phase, deviate significantly from the pattern reported by Huang et al. and accordingly also from the patterns of MOF-5_n and MOF-5_m. The intensities of the first (6.9°, corresponding to a *d* of 12.8 Å) and second (9.7°, corresponding to a *d* of 9.1 Å) peak are inverted. Moreover, as the larger crystals of MOF-5_m give less peak broadening, finer details are revealed, and it is evident that the peak at 9.7° consists of two distinct contributions. The same peak splitting phenomenon can also be discerned for MOF-5_n from a pattern obtained using synchrotron radiation (Supporting Information Figure S2).

3.2. Thermal stability. Figure 3 displays a temperature resolved series of powder XRD patterns of the MOF-5_n sample. Clearly, the crystallinity remains virtually unaltered in the temperature range 75−350 °C, and a further temperature increase leads to a gradual transition to ZnO.

(23) Filipponi, A.; Borowski, M.; Bowron, T.; Ansell, S.; Di Cicco, A.; De Panfilis, S.; Itie, J. P. *Rev. Sci. Instrum.* **2000**, *71*, 2422−2432.
(24) Lamberti, C.; Bordiga, S.; Bonino, F.; Prestipino, C.; Berlier, G.; Capello, L.; D'Acapito, F.; Xamena, F. X. L. I.; Zecchina, A. *Phys. Chem. Chem. Phys.* **2003**, *5*, 4502−4509.
(25) Lamberti, C.; Prestipino, C.; Bordiga, S.; Berlier, G.; Spoto, G.; Zecchina, A.; Laloni, A.; La, Manna, F.; D'Anca, F.; Felici, R.; D'Acapito, F.; Roy, P. *Nucl. Instrum. Methods Phys. Res., Sect. B* **2003**, *200*, 196−201.
(26) Comin, F.; Incoccia, L.; Mobilio, S. INFN Frascati Laboratory Internal Report LNF-82/019(NT); INFN 1982.
(27) James, F.; Roos, M. *Comput. Phys. Commun.* **1975**, *10*, 343−367.
(28) James, F. *MINUIT Function Minimization and Error Analysis, Reference Manual*, version 94.1; CERN: Geneva, Switzerland, 1998.
(29) Ankudinov, A. L.; Ravel, B.; Rehr, J. J.; Conradson, S. D. *Phys. Rev. B* **1998**, *58*, 7565−7576.
(30) Prestipino, C.; Regli, L.; Vitillo, J. G.; Bonino, F.; Damin, A.; Lamberti, C.; Zecchina, A.; Solari, P. L.; Kongshaug, K. O.; Bordiga, S. *Chem. Mater.*, **2006**, *18*, 1337−1346.
(31) West, A. R. *Solid State Chemistry and its Applications*; John Wiley & Sons: New Delhi, India, 1992.
(32) Bordiga, S.; Vitillo, J. G.; Ricchiardi, G.; Regli, L.; Cocina, D.; Zecchina, A.; Arstad, B.; Bjørgen, M.; Hafizovic, J.; Lillerud, K. P. *J. Phys. Chem. B* **2005**, *109*, 18237−18242.

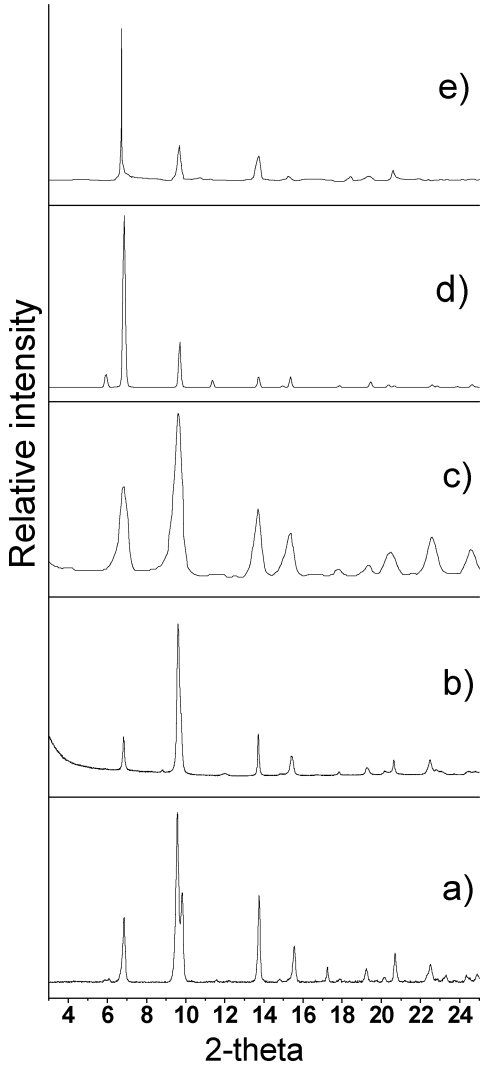

Figure 2. XRD patterns of (a) MOF-5_m and (b) MOF-5_n, (c) digitalized powder XRD pattern of MOF-5 obtained by Huang et al.,[7] (d) simulated powder XRD pattern for MOF-5, and (e) digitalized powder XRD pattern of MOF-5 obtained by Yaghi et al.[13]

However, an intensity increase of the 6.9° peak can be seen from the inset and this is related to pore-filling effects induced by solvent removal (see section 3.3 for further details). The desorption of the solvent and the thermal stability of the MOF-5_n was further examined by thermogavimetry combined with mass spectrometry (TG−MS), (Supporting Information S4) and transmission FTIR spectroscopy (Supporting Information S5). The TGA curve and its first derivative are reported in Figure 4. The inset in the figure shows a 2% weight loss in the temperature range 20−80 °C (seen as a distinct step in the first derivative plot). This weight loss is assigned to desorption of surface adsorbed water from parallel MS analysis. The next weight loss of about 18.5% is observed in the range 80 to 240 °C, and represents elimination of DMF. A complete removal of the solvent upon heating to 250 °C was also confirmed by FTIR spectroscopy (Supporting Information S5). Finally, a rather sharp weight loss of about 36.8% takes place after 375 °C and corresponds to the structural decomposition (see Supporting Information). The residue of the heated sample was proved to be ZnO by powder XRD (Figure 3).

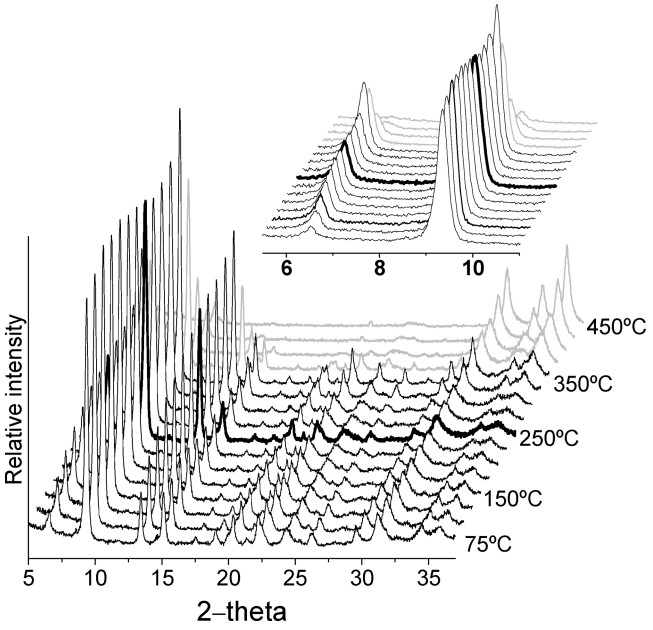

Figure 3. Series of temperature resolved powder XRD patterns of MOF-5_n. The gray patterns represent the transition from the MOF to ZnO. The inset shows the intensity details of the two peaks at the lowest 2θ angles.

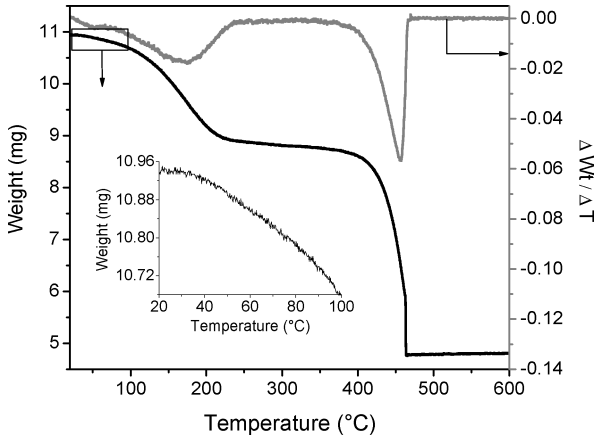

Figure 4. Thermogravimetric curves (as recorded and its first derivative) of MOF-5_n heated (5 °C/min) in O_2.

In summary, both temperature resolved powder XRD and TG−MS confirm that the MOF-5_n material has the same well-known high-thermal stability as the originally reported MOF-5.[11]

3.3. Structure Determination. The characterizations we have carried out so far essentially confirm that MOF-5_n and MOF-5_m are nearly indistinguishable from the material obtained by Huang et al.[7] The disagreement between the powder patterns of MOF-5_m/MOF-5_n and the calculated MOF-5 pattern (Figure 2) can be explained from single-crystal data.

The single-crystal data were collected for more than 10 different crystals of MOF-5_m because of the poor diffraction of several crystals at high 2θ angles. During this procedure two different kinds of MOF-5_m crystals were discovered, hereafter denoted MOF-5_m_Zn and MOF-5_m_int.

Figure 5 presents results from the structure solution of MOF-5_m_Zn. The framework obviously consists of the same building units as the originally reported MOF-5.[11] However, in MOF-5_m_Zn an additional electron density can be observed in the center of the small cages (i.e., the half of the cages where the

Table 1. Summary of Crystal and Refinement Data for the MOF-5_m Structures

		MOF-5_m_int	
	MOF-5_m_Zn	(room temp measurement)	(300 °C measurement)
empirical formula[a]	$C_{24}H_{12}O_{13}Zn_4$	$C_{24}H_{12}O_{13}Zn_4$	$C_{24}H_{12}O_{13}Zn_4$
cryst size (mm^3)	0.08 × 0.08 × 0.08	0.1 × 0.1 × 0.1	0.1 × 0.1 × 0.1
cryst syst	trigonal	trigonal	trigonal
space group	$R\bar{3}m$	$R\bar{3}m$	$R\bar{3}m$
a (Å)	18.406(10)	18.382(12)	18.452(6)
c (Å)	44.75(5)	44.97(2)	44.933(6)
V ($Å^3$)	13129(17)	13159(13)	13249(6)
Z	6	12	12
ρ ($Mg\ m^{-3}$)	0.584	1.166	1.158
λ (Å)	0.71073	0.38745	0.38745
θ range (deg)	2.21−19.05	1.48−12.62	1.21−14.01
T (K)	293(2)	293(2)	573(2)
abs coeff (mm^{-1})	1.103	1.158	1.151
measured reflns	16367	24083	61633
independent reflns	1344 [R_{int} = 0.1506]	2067 [R_{int} = 0.0995]	3294 [R_{int} = 0.0895]
data/restrains/params	1344/0/79	2067/0/159	3296/0/157
R1 [$I > 2\sigma(I)$][b]	0.0823 [0.1181]	0.0575	0.0374
wR2 [all data][b]	0.2401 [0.3603]	0.1421	0.1201
F^2(GOF)[b]	1.100 [1.417]	1.089	1.163
largest diff. peak and hole	0.595 and −0.938 e•A^{-3}	0.716 and −1.345 e•A^{-3}	0.793 and −1.280 e•A^{-3}

[a] For the framework only. [b] Statistics for non-SQUEEZED data are bracketed.

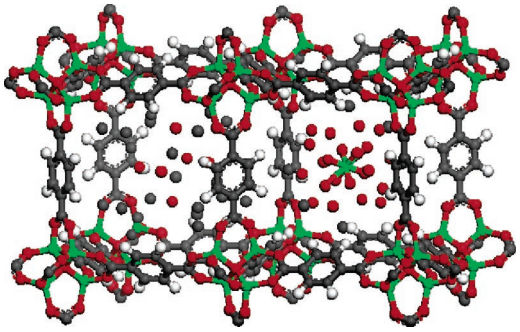

Figure 5. MOF-5_m_Zn with Zn cluster in the small cage and unorganized solvent in the large cage; the electron densities are illustrated with partly occupied oxygen and carbon atoms. Zn atoms are shown in green, O in red, C in gray, and H in white.

benzene rings are twisted into the cage center). This electron density has twice the intensity of a fully occupied oxygen atom. The best refinement was obtained by assigning the electron density to a Zn atom with occupancy of 0.5. The coordination sphere of the Zn atom consists of partially occupied oxygen positions. The structure data from the species in the cavities have large uncertainties, but the Zn−O distances are as expected for a $[Zn(OH)_2(H_2O)_2]$ or a $[Zn(NO_3)^2{\cdot}2(H_2O)_2]$ complex.[33] Zn−O distances in the range 2.0−2.2 Å are observed, and Zn appears to be eight coordinated, but this is probably due to two superimposed Zn atoms with tetrahedral coordination. It is not possible to discriminate between a nitrate cluster and a hydroxide cluster based on the XRD data alone. Also the nitrate group and DMF are undistinguishable. The Zn species in the pores were tentatively ascribed to $Zn(NO_3)_2{\cdot}(H_2O)_2$. A TG−MS reference analysis of pure $Zn(NO_3)_2{\cdot}6H_2O$ (not reported) showed that NO_2 gas evolves in the temperature range of 200−300 °C. NO_2 could not be detected in the parallel TG−MS analysis of the MOF, making it unlikely that $Zn(NO_3)_2$ are present. It is thus plausible that the additional electron densities represent $Zn(OH)_2$. The presence of OH groups after solvent removal at

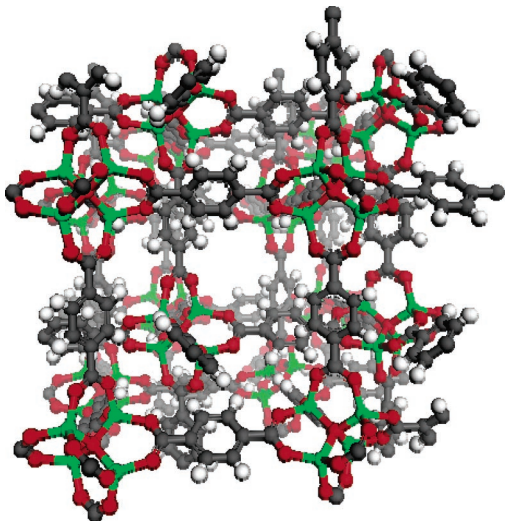

Figure 6. Structure of MOF-5_m_int solved from single-crystal XRD data recorded at 300 °C. Zn atoms are shown in green, O in red, C in gray, and H in white.

250 °C could also be discerned as a broad ν(OH) band in the FTIR spectrum (Supporting Information S5).

The experimental data of MOF-5_m_Zn suggested space-group $R\bar{3}m$ (No. 166), and the structure was solved and refined in this symmetry. The original MOF-5 structure was solved in the cubic symmetry ($Fm\bar{3}m$ No. 225), but the experimental data indicated that cubic symmetry was wrong for our structure (R_{sym} for the cubic lattice was 24% compared to 10% for the trigonal lattice). A summary of data related to the structure and refinement is presented in Table 1, while further details are given in Supporting Information. In all symmetries except $P1$, the Zn atom in the cavity is located in a special position. Our experience is that the occupancy of atoms in special positions is more susceptible to errors than atoms in general positions. The refinement was therefore repeated in $P1$ symmetry. An additional motivation to do a refinement in low symmetry was to identify a possible organization of the solvent arising from solvent−lattice interactions. This is often seen in zeolites[34] and

(33) Eriksson, L.; Louër, D.; Werener, P.-E. *J. Solid State Chem.* **1989**, *81*, 9−20.

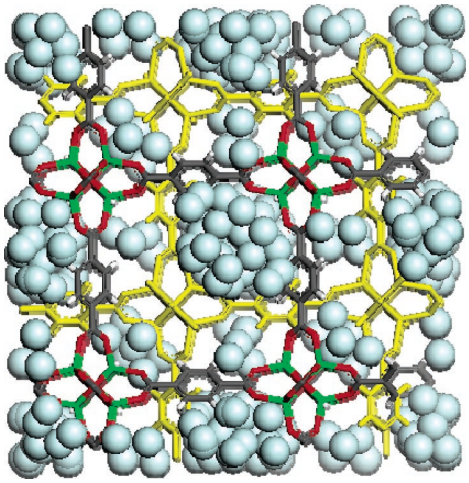

Figure 7. Structure of MOF-5_m_int solved from single-crystal XRD data recorded at room temperature. Distorted solvent is presented in a space-filling mode. The second MOF-5 lattice is drawn in yellow for the sake of clarity. Zn atoms are shown in green, O in red, C in gray, and H in white.

may give valuable information about how the solvent interacts with the lattice and thereby direct the crystallization process. However, the solvent confined inside the MOF cages seems to be totally random, indicating weaker lattice−solvent interactions compared to what we observe for more charged zeolite lattices. We were not able to obtain a satisfactory refinement in $R\bar{3}m$ with a model that includes a large amount of disordered solvent. The contribution from the solvent volume to the observed intensities was therefore subtracted from the original data by applying the SQUEEZE subroutine of PLATON,[35] which led to acceptable final residual values. Information about the MOF-5_m_Zn structure before being subjected to SQUEEZE is given in square brackets in Table 1. The solvent accessible volume in MOF-5_m_Zn is considerably larger than the recommended maximum value for the SQUEEZE subroutine, but it still performed adequately as long as all atoms in the solvent volume were excluded, as exemplified by the good agreement between the number of electrons accounted for by SQUEEZE and the number of electrons in solvent molecules and the Zn cluster. The information about the Zn cluster is extracted from the pre-SQUEEZE and the *P*1 refinements. After removal of the species in the cavities the symmetry may be increased, and 0.25 Å tolerance will change the symmetry from $R\bar{3}m$ (No. 166) to the original cubic MOF-5 symmetry ($Fm\bar{3}m$, No. 225). Thus, a clear consequence of the presence of the Zn clusters in the nanocavities is the symmetry change from cubic to trigonal.

Figure 6 illustrates the structure of MOF-5_m_int after removal of the solvent by heating to 300 °C, the same temperature at which the single-crystal data were recorded. MOF-5_m_int consists of two MOF-5 frameworks interpenetrated with each other. The frameworks are not physically connected, but there is sufficient interaction to cause a significant distortion of the cell from cubic to trigonal. R_{int} for the cubic lattice was 50% compared to 10% for the trigonal lattice. In the space group $R\bar{3}m$ the networks are related by symmetry. The structure was therefore also refined in the lower symmetry to allow for a separate occupation of the two networks. However, the best refinement was obtained with equal occupation. A

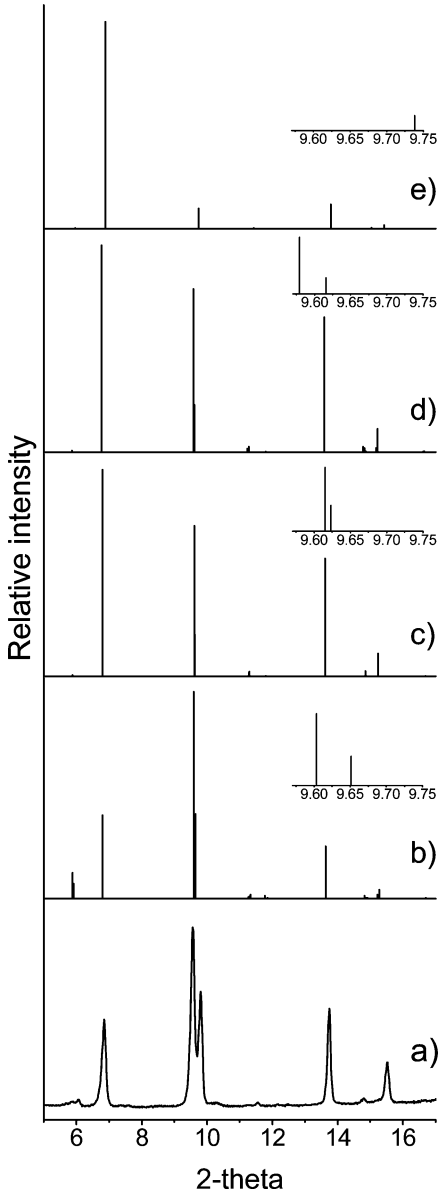

Figure 8. (a) Powder XRD pattern of MOF-5_m and calculated patterns of (b) MOF-5_m_Zn, (c) MOF-5_m_int with solvent in the pores, (d) MOF-5_m_int without solvent in the pores, and (e) original MOF-5 when transformed from cubic to trigonal symmetry. The insets show an expanded view of the 9.55−9.75 2θ range.

summary of data related to the structure and refinement is presented in Table 1, while further details are given as Supporting Information.

Figure 7 presents the structure of MOF-5_m_int with solvent molecules in the pores. DMF molecules cannot be localized in the refinement (this is again probably a result of disorder in the solvent), and they are therefore represented by dummy atoms to illustrate the electron density. The amount of the residual electron density in the Fourier difference map, representing the solvent, is also much lower than expected. The high energy beam generated by the synchrotron radiation heated the crystal and partially evaporated the solvent. However, diffuse electron densities placed in the middle of the pores can still be observed.

It is generally observed that for the materials with large voids accessible to solvent and adsorbates, the intensities of the XRD-reflections, particularly at low 2θ angles, are highly dependent on the amount and scattering power of the species present in

(34) McCusker, L. B.; Baerlocher, C.; Jahn, E.; Buelow, M. *Zeolites* **1991**, *11*, 308−313.
(35) Spek, A. L. *J. Appl. Crystallogr.* **2003**, *36*, 7−13.

the pores. It is known from the zeolites that removing water and cations from the pores strongly increases the relative intensities of the first reflections (Faujasite is a material that demonstrates this behavior particularly clearly). This effect is expected to be even more pronounced for MOF-type materials, where the species located in the pore volumes often account for an even larger fraction of the total mass. The most striking difference in the powder XRD patterns of the original MOF-5[11] and the MOF-5 reported by Huang et al. [7] (or MOF-5_n/MOF-5_m) is the strong shift in relative intensity of the low-angle reflections. Figure 8 compares the experimental powder XRD patterns of MOF-5_m (Figure 8a) with the patterns simulated for MOF-5_m_Zn (Figure 8b) and MOF-5_m_int (Figure 8c). For MOF-5_m_Zn, the second reflection (9.7°) is clearly strongest and in satisfying agreement with the experimental pattern of the bulk phase. Furthermore, the intensity of the reflection at 6.8° is strongly dependent on the amount of the pore filling material, whereas the reflection at 9.7° is unaffected. In a model with empty pores, the 9.7° reflection has lowest intensity. Filling the pores with DMF molecules (corresponding to the same amount of DMF calculated from the weight loss in the TG curve) increases the relative intensity of the reflection at 9.7° from 15 to 75%. The temperature-resolved series of powder patterns displayed in Figure 3 also shows a clear increase in intensity of the 6.8° reflection upon solvent removal. Further filling of the pores with the same amount of the $Zn(OH)_2$ species found in the *P*1 solution inverts the intensity of the peaks and strongly resembles the observed pattern for the bulk phase.

In the MOF-5_m_int phase, the second MOF-5 lattice can be regarded as a perfectly organized pore-filling material. Hence, the free pore volume created upon desolvation of the framework is no longer a main contributor to the scattering power. The intensity distribution in the powder XRD pattern is therefore not very sensitive to the amount of pore-filling material, and powder XRD patterns of MOF-5_m_int with and without solvent in the voids are very similar (Figure 8c and d). As the contribution of this phase is low (see later), the XRD pattern of the bulk phase is hardly affected by its presence.

The observed splitting of the peak at 9.7° proved to be a result of the distortion of the cubic symmetry. Comparison of the calculated patterns of MOF-5_m_Zn (Figure 8b) and MOF-5_m_int (Figure 8c) with the simulated pattern of the original MOF-5 (Figure 8e) structure, when transformed from cubic to trigonal symmetry (Figure S3), illustrates this. All patterns are simulated from trigonal structures, but only the one with the unit cell parameters calculated from the cubic cell lacks splitting of the 9.7° peak.

The reported unit cell parameters for MOF-5[11] and the unit cell parameters calculated from the obtained MOF-5_m pattern and from the structures solved from the single-crystal XRD are reported in Table 2. The extent of the distortion is reflected in the change of the axes lengths. The splitting is most evident in the pattern for the bulk phase where the deviation from the transformed trigonal cell is most significant.

In MOF-5_m_Zn the Zn−O species in the pores cause change in the axes lengths, while in the MOF-5_m_int the interaction between the two interpenetrated frameworks is responsible for the same effect. These results show that the large MOF-5 cell is highly flexible and allows significant changes in the unit cell axes without destroying the structure.

Table 2. The Unit Cell Parameters of the MOF-5 Materials

axes (Å)	cubic MOF–5 (with solvent)[2]	trigonal MOF-5 transformed from cubic	experimental MOF-5_m (indexed)	MOF-5_m_Zn	MOF-5_m_int
a	25.67	18.15	18.45	18.41	18.38
c	25.67	44.46	43.54	44.75	44.97

The single crystal and TG data were used to estimate what percent of the sample is constituted by MOF-5_m_Zn phase. The calculated weight loss for the desolvated, original MOF-5 upon decomposition is 58%, whereas the observed weight loss for MOF-5_m is 46%. This implies 12% excess of ZnO and corresponds to a MOF-5_m_Zn structure with one Zn species in every small cage. This is 50% more than the single-crystal data show, since the occupancy of the Zn species in the pores was refined to 0.5. Calculations based on the number of Zn atoms in the unit cells of both MOF-5_m phases, and the average number of Zn atoms in the unit cell calculated from TG data, show that our sample consists of 6% MOF-5_m_int. This accounts perfectly for the remaining 6% ZnO. Thus, the MOF-5_m sample consists of 94% MOF-5_m_Zn and 6% MOF-5_m_int.

The large deviation in the surface area of the original MOF-5 and MOF-5_m is due to Zn species in the pores. The presence of the nonvolatile compounds makes the host cavity inaccessible and may also block the entrance to the adjacent cavities. The estimated size of the Zn species is 7.5 Å (extracted from *P*1 structure solution), and the aperture joining the two cavities is approximately 8 Å. In addition, the minor phase consisting of doubly interpenetrated MOF-5 networks will also reduce the adsorption capacity.

The adsorption measurements have shown a higher Langmuir surface area for the MOF-5_m than for the MOF-5_n sample (see Section 3.1), implying less amount of $Zn(OH)_2$ species trapped in the pores. The adsorption properties are indeed in compliance with our powder XRD data (Figure 2), which illustrate a higher intensity of the 6.8° reflection for the MOF-5_m sample.

Finally, crystallization of the Zn species in the pores and interpenetration of networks explain also why the observed solvent related weight loss (18%) in the TG measurement is much lower than the estimated value (55−61%) for the space accessible to guest species in the MOF-5.[11]

3.4. EXAFS and XANES Characterization. The structure solutions of the MOF-5_m crystals revealed that the pores are occupied with highly disordered solvent molecules and Zn species. To extract more information about these virtually amorphous Zn species and the influence of dehydration and solvent removal on the first coordination sphere of Zn, the samples were further investigated with EXAFS. The EXAFS measurements were recorded for both MOF-5_m and MOF-5_n and the data are in general very similar, and only small variations associated with the crystallinity are observed. The raw XANES and EXAFS data are reported in Figure 9, and because of the similarity between the two sets of spectra, the detailed EXAFS analysis is only presented for MOF-5_m (Figure 10 and Table 3).

Figure 9a reports the XANES data whereas the EXAFS data are presented in Figure 9b. The data were obtained for both as

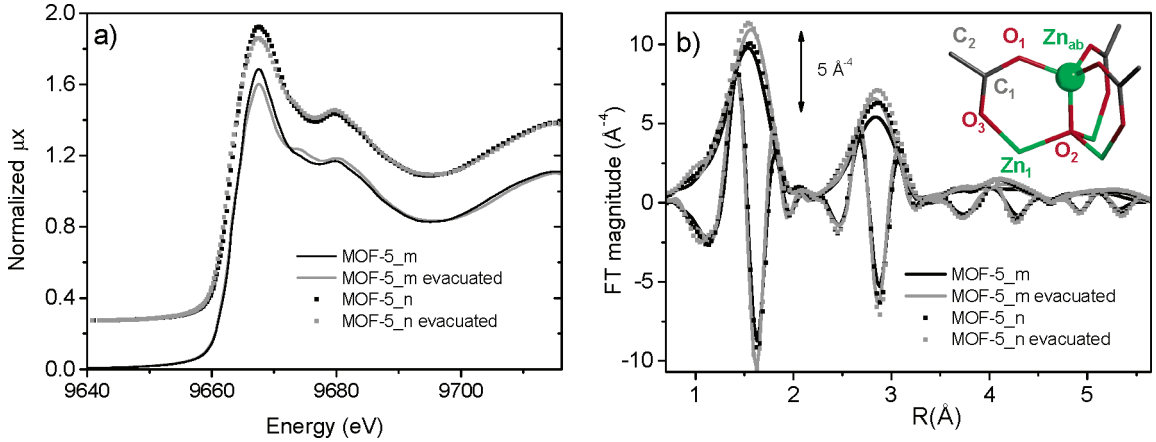

Figure 9. XAS data of MOF-5_m (solid line) and MOF-5_n (dotted line). The spectra of the as synthesized samples are drawn in black, whereas the spectra of the pretreated (vacuum at 250 °C) samples are drawn in gray. Panel a is the XANES region; the spectra representing MOF-5_n have been vertically shifted by 0.27 in normalized μx units. Panel b shows the k^3-weighted, phase uncorrected, EXAFS Fourier transformed signals (both modulus and imaginary parts). The inset in panel b shows the cluster used for EXAFS data analysis. Color code as in Figures 5−7.

Table 3. Parameters Obtained by Final Optimization of EXAFS Signals[a]

scattering path	type of scattering	*N*	*R* (Å)	σ^2 (Å^2)	ΔE_0 (eV)
$Zn_{ab}-O_1 + Zn_{ab}-O_2$	SS	4.9 ± 0.5	1.96 ± 0.01	0.006 ± 0.002	2.0 ± 2
$Zn_{ab}-O_{extra-phase}$	SS	1.1 ± 0.1	2.11 ± 0.01	0.008 ± 0.002	2.0 ± 2
$Zn_{ab}-C_1$	SS	3.7 ± 0.4	2.88 ± 0.02	0.008 ± 0.002	2.0 ± 2
$Zn_{ab}-C_1-O_1$	MS	7.4 ± 0.7	2.99 ± 0.02	0.008 ± 0.002	2.0 ± 2
$Zn_{ab}-Zn_1$	SS	3.7 ± 0.4	3.22 ± 0.02	0.009 ± 0.002	2.0 ± 2
$Zn_{ab}-C_1-O_3$	MS	3.7 ± 0.4	3.14 ± 0.02	0.008 ± 0.002	2.0 ± 2
$Zn_{ab}-O_3$	SS	3.7 ± 0.4	3.09 ± 0.02	0.006 ± 0.002	2.0 ± 2
$Zn_{ab}-O_1-C_2$	MS	7.4 ± 0.7	4.37 ± 0.03	0.013 ± 0.002	2.0 ± 2
$Zn_{ab}-Zn_1-O_1$	MS	7.4 ± 0.7	3.51 ± 0.03	0.015 ± 0.002	2.0 ± 2

[a] Coordination number (*N*); half of the path length, corresponding to the bond distance for SS contributions (*R*); Debye−Waller factors (σ^2) and energy shifts (ΔE_0). Owing to the small differences in the $Zn_{ab}-O_1$ and $Zn_{ab}-O_2$ distances, these two contributions have been simulated as a single contribution to the fit. Refer to the inset in Figure 9b for atom labeling. SS = single scattering; MS = multiple scattering.

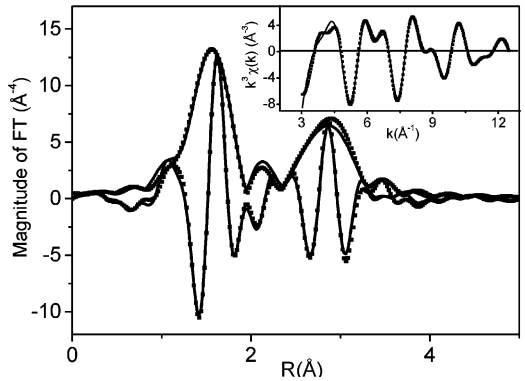

Figure 10. EXAFS analysis of outgassed MOF-5_m; experimental (scattered plot) and calculated (solid line) EXAFS k^3 weighted Fourier transform of filtered EXAFS signals (both modulus and imaginary parts). (Inset) Experimental (scattered plot) and calculated (solid line) Fourier back-transformed k^3 weighted EXAFS.

synthesized MOF-5_m and MOF-5_n and after pretreatment in vacuum at 250 °C. The vacuum pretreatment leads to some minor changes in the XANES edges (Figure 9a). Specifically, a shoulder appears at 9674 eV and the XANES white lines decrease. Further, the EXAFS signals (Figure 9b) display a general increase in intensity, as evidenced by the k^3 weighted EXAFS Fourier transformed signals of the two materials pretreated in vacuum at 250 °C. These small variations observed upon evacuation are supported by the crystallographic structure solution showing that the Zn species are coordinatively saturated. Thus, the removal of water and DMF should not have a direct influence on the coordinative sphere of Zn. The small modifications can be ascribed to the elimination of secondary interactions of solvent molecules with the first shell oxygen through hydrogen bonding.

A detailed analysis of the EXAFS signals of MOF-5_m was obtained by using the cluster in Figure 9b as a model for the local environment around Zn. During the analysis several constraints were applied in order to reduce correlation between different parameters. A single energy shift (ΔE_0) has been used for all paths. Moreover, similar paths were forced to have the same Debye−Waller (D−W) factor. The coordination number obtained by allowing eight different paths was kept proportional to the crystallographic data. Finally, an additional second coordination sphere of first oxygen was added to the optimization ($Zn_{ab}-O_{extra-phase}$ in Table 3). This strategy was adopted in order to take into account the presence of extra-framework species of the MOF-5_m_Zn phase. The obtained structural parameters are reported in Table 3, while the quality of the fit is evaluated from Figure 10. The quality of the fit is high and supported by the average bonding distance (1.96 ± 0.01) found with single-crystal XRD analysis. Moreover, a strong correlation between the coordination numbers and the D−W factors is observed. The contribution reported as $Zn_{ab}-O_{extra-phase,}$ was found to have bonding distance compatible with Zn−O distance in $Zn(OH)_2$ species occluded in the pores.

4. Conclusion

The scope of this report has been to shed light over the rather dramatic differences in adsorption properties and powder XRD data presented for MOF-5. The variations in surface area are accompanied by peak splitting and pronounced differences in the relative peak intensities in the powder XRD patterns. Single-crystal XRD was used to investigate the structural differences between low- and high-surface-area MOF-5. The low-surface-area MOF-5 sample had two different classes of crystals. $Zn(OH)_2$ species partly occupy the cavities of the dominant phase, making the hosting cavity and some of the adjacent cavities inaccessible for probe molecules. The minor phase consisting of doubly interpenetrated MOF-5 networks will also serve to lower the adsorption capacity. The presence of Zn-species and lattice interpenetration changes the symmetry from cubic to trigonal and explains the peak splitting observed in the powder XRD patterns. Pore filling effects from the Zn-species (and partly the solvent molecules) are also responsible for the pronounced variations in powder XRD peak intensities. The intensity ratios can be used diagnostically to predict the adsorption properties of a MOF-5-type material.

Acknowledgment. We are grateful for financial support from INSTM (Progetto PRISMA04) and from The Norwegian Research Council (Grants 160052/V30 and 158552/441). We also acknowledge the assistance from the staffs of the ESRF beamlines BM29 and ID31 (in particular P. L. Solari, M. Brunelli, and A. N. Fitch) throughout experiment CH-1700.

Supporting Information Available: Figure showing diffraction properties of MOF-5_m crystals; experimental powder XRD pattern of MOF-5_n recorded with synchrotron radiation; figure illustrating cell relations; details of MS and FTIR measurements; X-ray crystallographic files (CIF); details of EXAFS analysis. This material is available free of charge via the Internet at http://pubs.acs.org.

JA0675447